(Preprint) AAS 19-651

DESENSITIZED OPTIMAL ATTITUDE GUIDANCE FOR DIFFERENTIAL-DRAG RENDEZVOUS

Andrew Harris*, Ethan Burnett, and Hanspeter Schaub†

Growing interest in fuel-constrained small satellites, large Low Earth Orbit (LEO) constellations, and robustness to thruster failure has motivated the use of drag forces for orbit control. This work presents a novel method of achieving differential-drag formation flight using only attitude control and spacecraft geometry while desensitizing the control to uncertainties in atmospheric properties. This work applies and extends the theory of desensitized optimal control to the attitude-driven differential drag problem and derives new strategies for coping with systems whose control sensitivities are dependent on uncertain parameters. These new attitude guidance strategies are compared versus traditional LQR-based strategies in nominal cases and under the presence of large deviations in atmospheric density.

INTRODUCTION

Constellation- and formation-flight of spacecraft requires substantial on-board control effort and could benefit from the use of environmental forces, such as atmospheric drag, to conduct maneuvers in place of propellant-consuming thrusters. At present, the unpredictable nature of atmospheric drag due to the turbulent upper atmosphere has restricted the precision and utility of drag-based maneuvering. This work aims to apply sensitivity-minimization techniques to differential drag control to mitigate the coupling between uncertain environmental conditions and control results.

While controlling spacecraft using atmospheric forces has been proposed since the 1980s, uncertainty surrounding both atmospheric neutral density models and atmosphere-surface interaction has hampered its practical application. Neutral atmospheric density in LEO can vary by orders of magnitude depending on solar forcing, geomagnetic activity, and diurnal variation.[1] This alone presents a substantial challenge to using differential drag for regular space operations, and is further compounded by the limited progress that has been made in predictive modeling for atmospheric density.[2] While higher accuracy models are potentially possible by incorporating live density estimates–for example, by measuring orbit variations in tracked orbital debris, as shown by[3]–these models rely on the availability of high-accuracy tracking data and spacecraft drag models, which are not widely available. This limitation severely constraints the types of missions and applications for differential-drag control to those that can tolerate substantial uncertainty in control accuracy, settling time, and other performance indices.

*Research Assistant, Ann and H.J. Smead Department of Aerospace Engineering Sciences, University of Colorado Boulder, Boulder, CO, 80309 USA.

†Glenn L. Murphy Chair of Engineering, Smead Department of Aerospace Engineering Sciences, University of Colorado, 431 UCB, Colorado Center for Astrodynamics Research, Boulder, CO 80309-0431. AAS Fellow,AIAA Fellow.

While a variety of methods for leveraging atmospheric drag for spacecraft have been proposed ,[4–9] few have directly studied methods for mitigating the impact of mis-modeled atmospheric density. Time-optimal or bang-bang differential drag strategies can be naturally robust to these variations, as their control depends only upon the sign of the commanded acceleration rather than the magnitude;[10] however, their performance can vary considerably. Prior work in formulating the attitude-driven differential-drag formation control problem as a linear regulation problem[11] has also shown to be reasonably robust with respect to density variation. While these methods are robust to variation, their performance can vary significantly as the atmospheric density changes, thereby hampering mission operations that depend on relatively precise timing or positioning. This work aims to develop techniques for differential-drag control that minimize performance variation with respect to density changes.

Desensitized optimal control is a family of related techniques for minimizing the dependence of a given trajectory or control strategy to selected environmental parameters. Originating in the 1960s with the sensitivity-vector approach described by Kahne,[12] desensitized optimal control has been successfully applied in other fields, such as optimal landing guidance[13] and multi-body structures.[14] Seywald[15] presents a method for considering state sensitivities to system parameters by constructing a state transition matrix for those states and adding cost penalties for exciting those states, allowing the desensitized optimal control problem to be applied to general nonlinear problems. Makkapati[16] presents an alternative formulation using sensitivity functions, which are both similar to the original approach developed by Kahne and which offer improved computational efficiency versus the sensitivity matrix approach. This work develops an alternative derivation of the sensitivity-vector approach for linear systems that can be considered a restricted case of Makkapati's sensitivity function control.

This work is arranged as follows. First, a brief overview of the drag-perturbed linearized relative dynamics model and attitude effect is reviewed. Next, the theory of desensitized optimal control is reviewed and extended to consider sensitivities arising directly from control inputs. This extended methodology is then applied to the differential drag formation flying case, and demonstrated in simulation versus previously-shown static LQR controllers. Finally, Monte Carlo simulations demonstrating the impact of density uncertainty and measurement noise are presented to demonstrate the realized robustness of the desensitized approach.

PROBLEM STATEMENT

Differential drag formation flight is a long-standing technique for achieving in-plane formation control without the use of expensive, failure-prone thrusters. Prior work has shown that, given non-uniform geometries, attitude control alone is sufficient to achieve controllability between two spacecraft using differential drag.[11] The derived attitude-dependent linearized equations of motion take the form of the Hill-Clohessy-Wiltshire equations plus several drag terms dependent on the spacecraft ballistic coefficient as derived by Silva[17] and refined in Reference:[11]

$$\ddot{x} = 2\dot{y}n + 3n^2x - \frac{1}{2}\beta_d P_d n r_c \dot{x} \tag{1}$$

$$\ddot{y} = -2\dot{x}n - n^2 r_c^2 \frac{1}{2}(\beta_C P_C - \beta_d P_d) - \beta_d P_d n r_c \dot{y} \tag{2}$$

$$\ddot{z} = -zn^2 - \frac{1}{2}(\beta_d P_d r_c n)\dot{z} \tag{3}$$

The sensitivity of these equations with respect to the ballistic coefficient is taken from Reference[11] as:

$$\frac{\partial \ddot{x}}{\partial \boldsymbol{\sigma}_p} = -\frac{1}{2} P_d n r_c \dot{x}_0 \frac{\partial \beta_d}{\partial \boldsymbol{\sigma}_p} \tag{4}$$

$$\frac{\partial \ddot{y}}{\partial \boldsymbol{\sigma}_p} = (\frac{1}{2} n^2 r_c^2 P_d - P_d n r_c \dot{y}_0) \frac{\partial \beta_d}{\partial \boldsymbol{\sigma}_p} \tag{5}$$

$$\frac{\partial \ddot{z}}{\partial \boldsymbol{\sigma}_p} = -\frac{1}{2} (P_d r_c n) \dot{z}_0 \frac{\partial \beta_d}{\partial \boldsymbol{\sigma}_p} \tag{6}$$

and the derivative of the ballistic coefficient with respect to attitude (which is defined in terms of MRPs for their amicable linearization) for a faceted spacecraft with constant drag coefficients across each facet is taken from Reference[11] to be

$$\frac{\partial \beta_d}{\partial \boldsymbol{\sigma}_p} = \frac{1}{m_i} \sum_{i=1}^{n} -4 C_{D,i} A_i \hat{\boldsymbol{n}}_i{}^T \frac{\partial}{\partial \sigma_p} ([\boldsymbol{\sigma}_p \times][BN(\boldsymbol{\sigma}_r)] \hat{\boldsymbol{v}}) \tag{7}$$

While these equations are linear in both the relative states and the linearized MRPs, both the state dynamics and the control effects contain an implicit dependence on the time-varying neutral density, P_d, and the chief radius and mean motion, r_c and n respectively. These parameters vary as drag acts to reduce the orbital radius of the chief and deputy alike, representing a source of modeling error within the dynamics.

Atmospheric Model

For the purposes of this work, a simple exponential atmospheric model is used for the controller's design due to its analytical form. Exponential atmospheric models have the following form:

$$\rho = \rho_0 \mathrm{e}^{-\frac{|\boldsymbol{r} - \boldsymbol{r}_E|}{h}} \tag{8}$$

where $\boldsymbol{r}$ is the inertial, Earth-centric spacecraft position, $\boldsymbol{r}_E$ is the Earth's mean radius, ρ_0 is the atmospheric density at the Earth's surface, and h is the scale height of the atmosphere. In general, these properties are only coarsely known, and can vary substantially with changes in geomagnetic or solar weather.

DESENSITIZED OPTIMAL CONTROL

Desensitized optimal control is a subset of optimal control techniques that attempts to generate optimal control solutions or trajectories under the presence of perturbations in parameters. The methodology of Kahne[12] is briefly summarized here for reference, with an additional extension to sensitivities in the control matrix B.

As described by Kahne, the sensitivities of a linear system $\dot{\boldsymbol{x}} = [A]\boldsymbol{x} + [B]\boldsymbol{u}$ are best understood as the gradient of the system's state dynamics with respect to a parameter α:

$$\dot{\boldsymbol{s}} = \frac{\partial \dot{x}}{\partial \alpha} = [A]\boldsymbol{s} + [C]\boldsymbol{x},\ \boldsymbol{s}(0) = \boldsymbol{0} \tag{9}$$

where $[A]$ are the linear state dynamics, and the state sensitivity matrix $[C]$ is defined by $C_{ij} = \frac{\partial A_{ij}}{\partial \alpha}$. Notably, this expression ignores the dependence of the sensitivities upon the control inputs,[12]

which are assumed to be independent of the sensitivity parameter; however, if the control effects matrix is affected by the sensitivities, an additional matrix $[D]$ is introduced (similarly defined as $D_{ij} = \frac{\partial B_{ij}}{\partial \alpha}$), yielding the updated sensitivity dynamics:

$$\dot{\boldsymbol{s}} = [A]\boldsymbol{s} + [C]\boldsymbol{x} + [D]\boldsymbol{u} \tag{10}$$

Using this definition of the sensitivities, the objective of minimizing the overall system sensitivity is defined by the sensitivity cost

$$J_s = \int_{t_0}^{t_f} \boldsymbol{s}(t)^T \Sigma \boldsymbol{s}(t) dt \tag{11}$$

which can be readily combined with the classical LQR cost function to yield

$$J = \boldsymbol{x}_f^T N \boldsymbol{x}_f + \int_{t_0}^{t_f} \boldsymbol{x}(t)^T Q \boldsymbol{x}(t) + \boldsymbol{u}(t)^T R \boldsymbol{u}(t) + \boldsymbol{s}(t)^T \Sigma \boldsymbol{s}(t) \tag{12}$$

From this, the formal statement of the desensitized optimal control problem is stated as:

$$\begin{aligned} \underset{u}{\text{minimize}} \quad & J = \boldsymbol{x}_f^T N \boldsymbol{x}_f + \int_{t_0}^{t_f} \boldsymbol{x}(t)^T Q \boldsymbol{x}(t) + \boldsymbol{u}(t)^T R \boldsymbol{u}(t) + \boldsymbol{s}(t)^T \Sigma \boldsymbol{s}(t) \\ \text{subject to} \quad & \dot{\boldsymbol{x}} = [A]\boldsymbol{x}(t) + [B]\boldsymbol{u}(t),\ \dot{\boldsymbol{s}} = [A]\boldsymbol{s}(t) + [C]\boldsymbol{x}(t) + [D]\boldsymbol{u}(t) \end{aligned}$$

The Hamiltonian for this problem is written using a separate set of co-states for each constraint, denoted $\boldsymbol{p}$ for the state dynamic constraint and $\boldsymbol{\lambda}$ for the sensitivity dynamics.

$$H = \boldsymbol{x}(t)^T Q \boldsymbol{x}(t) + \boldsymbol{u}(t)^T R \boldsymbol{u}(t) + \boldsymbol{s}(t)^T \Sigma + \boldsymbol{p}(t)^T ([A]\boldsymbol{x}(t) + [B]\boldsymbol{u}(t)) + \boldsymbol{\lambda}^T ([A]\boldsymbol{s}(t) + [C]\boldsymbol{x}(t) + [D]\boldsymbol{u}(t)) \tag{13}$$

The cannonical equations of this system are:

$$\begin{aligned} \dot{\boldsymbol{x}} &= \frac{\partial H}{\partial \boldsymbol{p}} = [A]\boldsymbol{x}(t) + [B]\boldsymbol{u}(t) \\ \dot{\boldsymbol{s}} &= \frac{\partial H}{\partial \boldsymbol{\lambda}} = [A]\boldsymbol{s}(t) + [C]\boldsymbol{x}(t) + [D]\boldsymbol{u}(t) \\ \dot{\boldsymbol{p}} &= -\frac{\partial H}{\partial \boldsymbol{x}} = -Q\boldsymbol{x} - [A]^T \boldsymbol{p} - [C]^T \boldsymbol{\lambda} \\ \dot{\boldsymbol{\lambda}} &= -\frac{\partial H}{\partial \boldsymbol{s}} = -\Sigma \boldsymbol{s} - [A]^T \boldsymbol{s} \end{aligned} \tag{14}$$

The control parameter, $\boldsymbol{u}$, can be solved for using the additional property

$$\frac{\partial H}{\partial u} = \boldsymbol{0} \tag{15}$$

which yields

$$0 = [R]\boldsymbol{u} + [B]^T \boldsymbol{p} + [D]^T \boldsymbol{\lambda} \tag{16}$$

$$\boldsymbol{u} = -[R]^{-1}([B]^T \boldsymbol{p} + [D]^T \boldsymbol{\lambda}) \tag{17}$$

Substituting this back into Equation 14 and collecting the terms yields the following total system dynamics matrix:

$$\begin{bmatrix} \dot{\boldsymbol{x}} \\ \dot{\boldsymbol{s}} \\ \dot{\boldsymbol{p}} \\ \dot{\boldsymbol{\lambda}} \end{bmatrix} = \begin{bmatrix} [A] & \boldsymbol{0} & -[B][R]^{-1}[B]^T & -[B][R]^{-1}[D]^T \\ [C] & [A] & -[D][R]^{-1}[B]^T & -[D][R]^{-1}[D]^T \\ -[Q] & \boldsymbol{0} & -A^T & -C^T \\ \boldsymbol{0} & -[\Sigma] & \boldsymbol{0} & -A^T \end{bmatrix} \begin{bmatrix} \boldsymbol{x} \\ \boldsymbol{s} \\ \boldsymbol{p} \\ \boldsymbol{\lambda} \end{bmatrix} \tag{18}$$

The initial conditions of this equation are given by:

$$\begin{aligned} \boldsymbol{x}(0) &= \boldsymbol{x}_0 \\ \boldsymbol{s}(0) &= \mathbf{0} \\ \boldsymbol{p}(t_f) &= F\boldsymbol{x}(t_f) \\ \boldsymbol{\lambda}(t_f) &= \mathbf{0} \end{aligned} \tag{19}$$

These equations form a linear system in time whose state transition matrix, Φ, can be solved for. The elements of this matrix are written in terms of the super-state, $\boldsymbol{z}(t) = \begin{bmatrix}\boldsymbol{x}(t) & \boldsymbol{s}(t)\end{bmatrix}^T$, and the adjoint super-state, $\boldsymbol{\psi}(t) = \begin{bmatrix}\boldsymbol{p}(t) & \boldsymbol{\lambda}(t)\end{bmatrix}^T$:

$$\begin{bmatrix}\boldsymbol{z} \\ \boldsymbol{\psi}\end{bmatrix} = \begin{bmatrix}\phi_{11}(t,t_0) & \phi_{12}(t,t_0) \\ \phi_{21}(t,t_0) & \phi_{22}(t,t_0)\end{bmatrix}\begin{bmatrix}\boldsymbol{z}_0 \\ \boldsymbol{\psi}_0\end{bmatrix} \tag{20}$$

From Kahne,[12] this matrix and its submatrices are invertable, allowing us to solve for the dynamics of the costates over time:

$$\boldsymbol{\psi}(t) = [\phi_{22}(T,t) - G\phi_{12}(T,t)]^{-1}[G\phi_{11} - \phi_{21}(T,t)]\boldsymbol{z}(t) = K(t)\boldsymbol{z}(t) \tag{21}$$

where $K(t)$ denotes the optimal linear feedback gain. Differentiating this equation with respect to time and substituting in the state and co-state dynamics yields a modified version of the Matrix Ricatti equation:

$$\dot{K}(t) + K(t)L(t) + P(t)K(t) - K(t)M(t)K(t) + N(t) = 0 \tag{22}$$

$$L(t) = \begin{bmatrix}[A] & \mathbf{0} \\ [C] & [A]\end{bmatrix} \tag{23}$$

$$P(t) = \begin{bmatrix}-A^T & -C^T \\ \mathbf{0} & -[A]\end{bmatrix} \tag{24}$$

$$M(t) = \begin{bmatrix}-[B][R]^{-1}[B]^T & -[B][R]^{-1}[D]^T \\ -[D][R]^{-1}[B]^T & -[D][R]^{-1}[D]^T\end{bmatrix} \tag{25}$$

$$N(t) = \begin{bmatrix}-[Q] & \mathbf{0} \\ \mathbf{0} & -[\Sigma]\end{bmatrix} \tag{26}$$

The optimal gain matrices are found by integrating this equation backwards in time from the terminal condition $K_{11}(t_f) = F\boldsymbol{x}(t_f)$; in terms of the gain matrix elements, this can be rewritten as a set of coupled ordinary differential equations:

$$\dot{K}_{11} = -K_{11}A - K_{12}C - A'K_{11} - C'K_{21} + K_{11}BR^{-1}B'K_{11} - Q \tag{27}$$

$$\dot{K}_{12} = -K_{12}A - A'K_{12} - C'K_{22} + K_{11}BR^{-1}B'K_{12} \tag{28}$$

$$\dot{K}_{21} = -K_{21}A + K_{22}C + A^TK_{21} - K_{21}BR^{-1}B^T \tag{29}$$

$$\dot{K}_{22} - -K_{22}A - A'K_{22} + K_{21}BR^{-1}B'K_{12} - \Sigma \tag{30}$$

Finally, the optimal closed-loop control trajectory is found using

$$\boldsymbol{u}(t) = -R^{-1}B(K_{11}(t)\boldsymbol{x}(t) + K_{12}(t)\boldsymbol{s}(t)) \tag{31}$$

Reachability and Controllability of Sensitivities

A critical consideration for the application of desensitized control to a system is whether the system sensitivities are adequately coupled to the states and control inputs such that they can be affected. Because both the state and sensitivity dynamics are linear and coupled, it is possible to construct an augmented system consisting of both the states and their corresponding sensitivities:

$$\begin{bmatrix}\dot{\boldsymbol{x}}\\ \dot{\boldsymbol{s}}\end{bmatrix} = \begin{bmatrix}[A] & \mathbf{0}_{n\times n}\\ [C] & [A]\end{bmatrix}\begin{bmatrix}\boldsymbol{x}\\ \boldsymbol{s}\end{bmatrix} + \begin{bmatrix}[B]\\ [D]\end{bmatrix}\boldsymbol{u} \tag{32}$$

This augmented system is itself a linear system and can therefore be analyzed with standard tools in linear controls. The reachable subspace of the system given the inputs can be computed by analyzing the system controllability matrix, $[O]$, for its rank (which reflects the number of controllable eigen-directions). Likewise, a basis for the controllable subspace can be found by analyzing the QR decomposition of $[O]$ and examining the first `rank(`O`)` columns.

APPLICATIONS

Mass-Spring-Damper with Force Control

The simplest example of a dynamical system with sensitivities to a coarsely-known parameter is a mass-spring-damper system with a variable mass. The equations of motion for this system assuming a linear spring and damper are given in state-space form as

$$[A] = \begin{bmatrix}0 & 1\\ -\frac{k}{m} & -\frac{c}{m}\end{bmatrix},\ \boldsymbol{x} = \begin{bmatrix}x\\ \dot{x}\end{bmatrix} \tag{33}$$

$$[B] = \begin{bmatrix}0\\ \frac{1}{m}\end{bmatrix},\ \boldsymbol{u} = \begin{bmatrix}F\end{bmatrix} \tag{34}$$

The sensitivity matrices are given by

$$[C] = \begin{bmatrix}0 & 0\\ \frac{k}{m^2} & \frac{c}{m^2}\end{bmatrix},\ [D] = \begin{bmatrix}0\\ -\frac{1}{m}\end{bmatrix} \tag{35}$$

To demonstrate the efficacy of the control-desensitized approach in comparison to prior methods, simulations were run across a range of mass values with 1 kilogram as the reference value. Figure 1 demonstrates how the control-desensitized and desensitized approach compare to a finite-time LQR solution at the design value and at an extreme mass value; the finite-time LQR approach produces much different behavior at the extremes, while the desensitized and control-desensitized approaches produce similar outcomes at varying values of the system mass.

To extend this comparison, the trajectory energy $\boldsymbol{x}^T\boldsymbol{x}$ was integrated over time at various values of mass; in these cases, reduced trajectory energy corresponds to faster system settling times, and is used as a comparative performance metric. The results, shown in Figure 2, show that the control-desensitized trajectories vary less with the uncertain parameter than the finite-time LQR or state-desensitized LQR approaches.

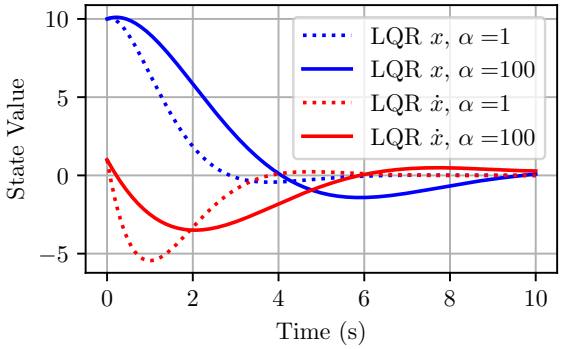

(a) Finite-Time LQR trajectory

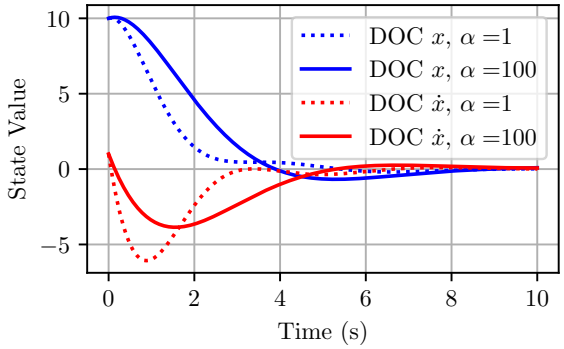

(b) Desensitized Trajectory

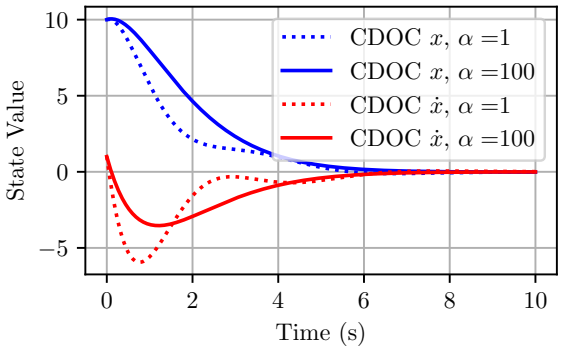

(c) Control-Desensitized Trajectory

Figure 1: State values versus time for nominal ($m = 1$) and off-nominal $m = 100$ LQR, DOC, and CDOC controllers for the spring-mass-damper system.

Differential Drag Formation Flight

Controlling relative spacecraft position and velocity with differential drag introduces a coupling between the system's controllability and the local atmospheric density, the latter of which is often only coarsely known. In addition, formulations that depend on knowledge of other orbital parameters, such as the Hill-Clohessy-Wiltshire derived differential drag formation flight system described by Eqn. 1-3, which are also coarsely-known. As such, these systems are prime candidates for the application of desensitized optimal control.

To maintain numerical conditioning of the resulting matrices, it is desirable for the magnitude of the sensitivity matrix to be on the same order as the state dynamics. Noting that the system is linear in many uncertain parameters–namely n, P_d, r_c, and the reference deputy ballistic coefficient β_d– we introduce an additional scaling parameter α on these quantities, and seek to minimize our sensitivity to variations in α. This is equivalent to minimizing the sensitivity of the system to any of the designated values, but without the potential for numerical conditioning issues. Incorporating

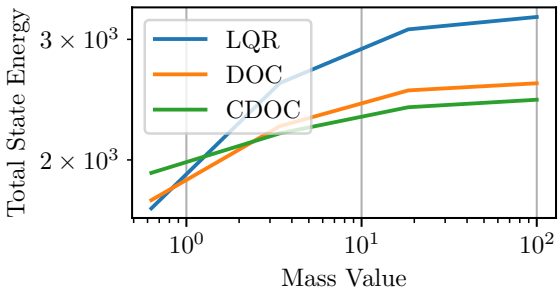

Figure 2: Trajectory energy vs. system mass for LQR, DOC, and CDOC controllers.

this additional parameter and reducing the state dynamics to the in-plane controllable states yields

$$A = \frac{\partial F}{\partial \boldsymbol{x}} = \begin{bmatrix} 0 & 0 & 1 & 0 \\ 0 & 0 & 0 & 1 \\ 3n^2 & 0 & \frac{1}{2}\alpha\beta_d P_d n r_c & 2n \\ 0 & 0 & -2n & -\alpha\beta_d P_d n r_c \end{bmatrix}, [C] = \frac{\partial A}{\partial \alpha} = \begin{bmatrix} 0 & 0 & 0 & 0 \\ 0 & 0 & 0 & 0 \\ 0 & 0 & \frac{1}{2}\beta_d P_d n r_c & 0 \\ 0 & 0 & 0 & -\beta_d P_d n r_c \end{bmatrix} \tag{36}$$

$$D = \frac{\partial B}{\partial \alpha} = \begin{bmatrix} \mathbf{0}_{3\times 3} \\ 0 \\ \frac{1}{2}n^2 r_c^2 P_d \frac{\partial \beta_d}{\partial \boldsymbol{\sigma}_p} \\ 0 \end{bmatrix}, \boldsymbol{u} = \begin{bmatrix} \sigma_{p,1} \\ \sigma_{p,2} \\ \sigma_{p,3} \end{bmatrix} \tag{37}$$

where $\alpha_{\text{nom}} = 1$ is used to maintain numerical conditioning. From these expressions, it is apparent that the sensitivity of the system to variations in the presumed environmental parameters results directly from the amplitude of the planar relative velocity and the spacecraft's attitude variation.

This information maps to the dynamics of attitude-driven differential drag, as the matrix elements for those states arise directly from the drag-coupled dynamics terms. $[C]$, which represents the mapping from states to sensitivities, has two marginally stable eigenvalues, one stable one, and one unstable eigenvalue. Likewise, these matrices show that the dominant contributors to the system's sensitivity to variations in atmospheric density are the planar velocity states and the control input attitude. In this sense, the derived $[C]$ and $[D]$ matrices provide analytical insight into the sources of uncertainty within the system, thereby providing designers with additional information for heuristic maneuver planning or formation design.

Expected Controllability

While the in-plane relative states are known to be controllable, the sensitivities of those states must be examined. To do so, the augmented linear system described by Eqn. 32 is constructed for the desensitized differential drag system described by Eqns. 36-37. The results of this analysis are shown in Table 1, and show that while the in-plane states remain controllable as expected, only the radial position sensitivity (s_1) is controllable given the assumed input. Uncontrollable eigendirections exist in both the y-position sensitivity s_2 and the planar velocity sensitivities s_3 and s_4, though these states are partially controlled through a coupling to the planar velocities.

Table 1: Controllability analysis results.

Control Type	$\texttt{Rank}([O])$
LQR	4
DOC	5
CDOC	5

PERFORMANCE CHARACTERIZATION

Prior work has shown control results for this system using LQR-based control using static gains. This approach is used as a baseline with which the optimal control techniques described in Section can be compared. To this end, three specific guidance approaches are demonstrated:

1. Finite-time LQR
2. Desensitized optimal control w/o control dependence
3. Desensitized optimal control with control dependence

These strategies are compared in a semi-realistic design environment, in which the control gains are designed on the linear differential drag model described by Equations 36–37 but simulated using the nonlinear equations for two-body dynamics plus a facet-based drag model; for more details on the propagation environment, see Reference 11.

To provide apples-to-apples comparisons, solution-specific results such as the overall cost are not presented; additionally, each controller was tuned individually using combinations of state, control, sensitivity, and final error weights. The final values used for each controller are listed in Table 3. Additionally, the initial conditions for the control scenario–designed to represent a 500 meter along-track maneuver in LEO – are listed in Table 2. The environmental and spacecraft parameters used are listed in Table 4.

Table 2: Orbital elements for both the deputy and chief spacecraft.

Orbital Element	Chief Value	Deputy Value
a	230km + r_{eq}	230km + r_{eq}
i	45°	$45.^\circ$
e	0	0
Ω	20.0°	20.0°
ω	30.0°	$30.0\ ^\circ$
M_0	20.0°	19.99°

Table 3: Selected control gains each strategy.

Control Design Variable	LQR	Desensitized Optimal	Control-Desensitized Optimal
Q	1.3	1	2
R	1e7	1e7	1e8
U	0	8e2	5e-5
N	1	1	1

Table 4: Spacecraft and environment parameters.

Parameter	Value
ρ_0	$1.020\ \frac{\text{kg}}{\text{m}^3}$
h	$8,000\text{m}$
A_i	$2\ \text{m}^2$
m_i	$6\ \text{kg}$
$C_{d,i}$	2.2

Linear Results

To demonstrate these results, controllers were evaluated for a 1-km slot-hopping maneuver using the linear dynamics. The state and state sensitivity results show that, while the states converge to the reference value, some sensitivity states either do not converge or retain oscillations relating to the described uncontrollable modes.

First, Hill-frame trajectories are displayed in Figure 6, with time histories of both the relative position and velocity trajectories shown in Figure 7. From these, note that the LQR and Control-Desensitized approaches both appear to successfully drive the deputy spacecraft to the origin in roughly 10-15 orbits, while the Desensitized approach merely moves the spacecraft towards the origin and prefers to minimize the initial motion of the spacecraft.

In comparing the LQR and Control-Desensitized approaches, it is apparent in looking at Figure 7a and Figure 7c that the control-desensitized approach produces much smaller relative velocities than the LQR-derived approach while achieving the same control objective in similar time; however, oscillations remain present in the Control-Desensitized trajectory that are damped out in the pure-LQR guidance approach. These results reflect a fundamental trade-off in the application of desensitized optimal control; in cases where control authority is limited, including penalties for sensitivities in the cost function J necessarily reduces the control's performance in the states. In addition, comparing the linear and nonlinear results suggests that the control-desensitized optimal controller and to a lesser extent the standard desensitized optimal controller appear to produce trajectories that resemble those generated by the linear system. To quantify this, the following non-linearity index is utilized:

$$\nu(t, t_0) = \frac{1}{t - t_0} \int_{t_0}^{t} \frac{||\boldsymbol{x}_{nl}(t) - \boldsymbol{x}_l(t)||}{||\boldsymbol{x}_l(t)||} dt \tag{38}$$

where $\boldsymbol{x}_{nl}(t)$ is the state propagated by the true nonlinear system and $\boldsymbol{x}_l(t)$ is the state propagated by the linear system. This metric was evaluated for all three controllers throughout the simulated maneuver; the resulting plot is shown in Figure 10. Here, it is apparent that the control-desensitized approach reduces the impact of nonlinearities on the system trajectory arising from the sensitivities.

ROBUSTNESS CHARACTERIZATION

Robustness Metrics and Methodolgy

For the purposes of this study, two performance metrics are used as figures of merit to compare the performance of the three outlined control strategies:

1. Terminal miss distance/velocity

2. Terminal and maximum nonlinearity indices

Exponential Atmosphere Parameter Changes

To demonstrate the performance of the CDOC and DOC control strategies on their proposed primary merit–reducing the variability of control performance with respect to density variation–two scenarios are examined under density variation: the 500m along-track maneuver of the previous section, where each control avoids the specified attitude boundaries and reaches the objective; and a 1500m along-track, 100m radial maneuver with the same gains where the control must encounter the linearity constraints to succeed. This allows us to compare the control strategies both at their designed performance and at the limit of their feasibility.

500m Along-Track Maneuver: Variation in the density of the atmosphere is a primary driver for uncertainty in differential drag formation flight and a key motivator for this work. To validate that this strategy indeed reduces the uncertainty associated with variable atmospheric density, the maneuver described in Section was simulated over a range of values for the base exponential density reflective of variation within LEO. In general, all of the control strategies remain convergent across density values; however, both the finite-time LQR control and the DOC control produce trajectories with wide variation from their linear predictions, while the CDOC strategy remains relatively close to the linear prediction despite large differences in atmospheric density. At the same time, the CDOC strategy is notably less accurate across the span of densities, though it still produces sub-meter positioning accuracy and sub-millimeter per second velocity accuracy. This loss of accuracy for the DOC and CDOC strategies again reflects the fundamental tradeoff between state and sensitivity performance described in Section . While the CDOC results appear to be less precise than the DOC or LQR results, they are much more consistent with respect to density variation, producing approximately the same terminal miss distances and velocities at 0.5 and 3 times the design density as at the reference.

From these analyses, it is evident that the control-desensitized approach produces slightly less accurate terminal position and velocity accuracy while remaining more consistent with its predicted linear trajectory across a range of density values. This is consistent with the theory of desensitized optimal control presented in Section . Notably, the control accuracy still produces sub-meter positioning accuracy and sub-millimeter-per-second velocity accuracy for the maneuver. This simulation represents a best-case scenario for each controller, which remains far from the linearity constraints imposed by the assumed attitude guidance input and converges relatively quickly given the allotted time; under these circumstances, the natural robustness of LQR-based control is apparent and the need for desensitization is reduced.

1500m Along-Track,100m Radial Maneuver: To better display the benefits of the CDOC approach, a larger maneuver based on the previous example was constructed by increasing the along-track separation to 2,500m and adding a radial offset of 100m. In the reference case, the LQR and DOC controllers reach the attitude saturation limit, but ultimately converge; the CDOC controller does not saturate, and converges before the other two. This more strenuous case was run over the same density range as the previous example, and the results are shown in Figures 13-14. In these cases, where the non-linearities in the system are more pressing, the control-desensitized strategy produces both better accuracy and less non-linearity than its competitors.

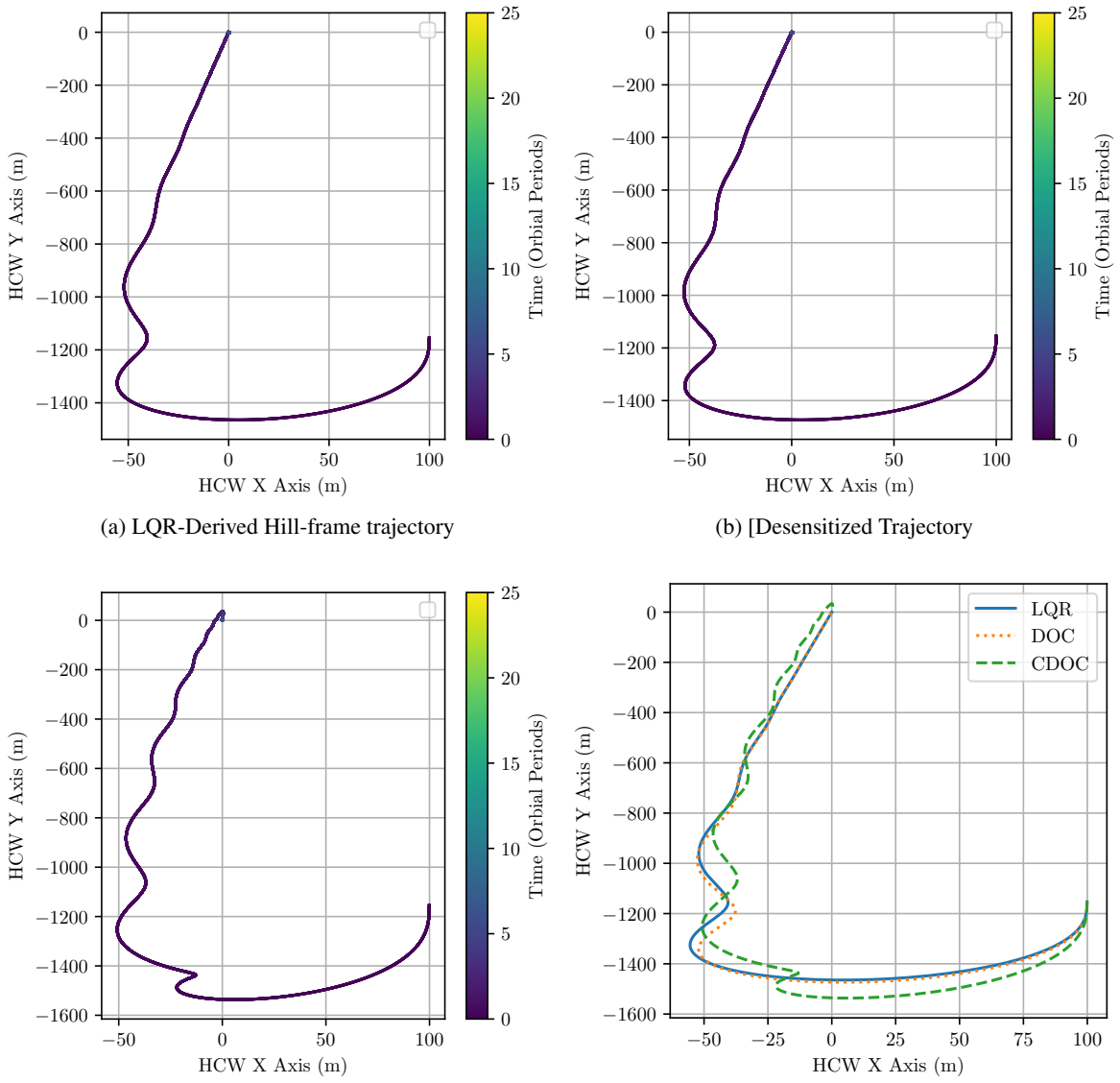

(a) LQR-Derived Hill-frame trajectory

(b) [Desensitized Trajectory

(c) Control-Desensitized Trajectory

(d) Comparison of static LQR, desensitized, and control-desensitized trajectories

Figure 3: Hill-frame performance of LQR, Desensitized, and Control-Desensitized Trajectories under linear dynamics

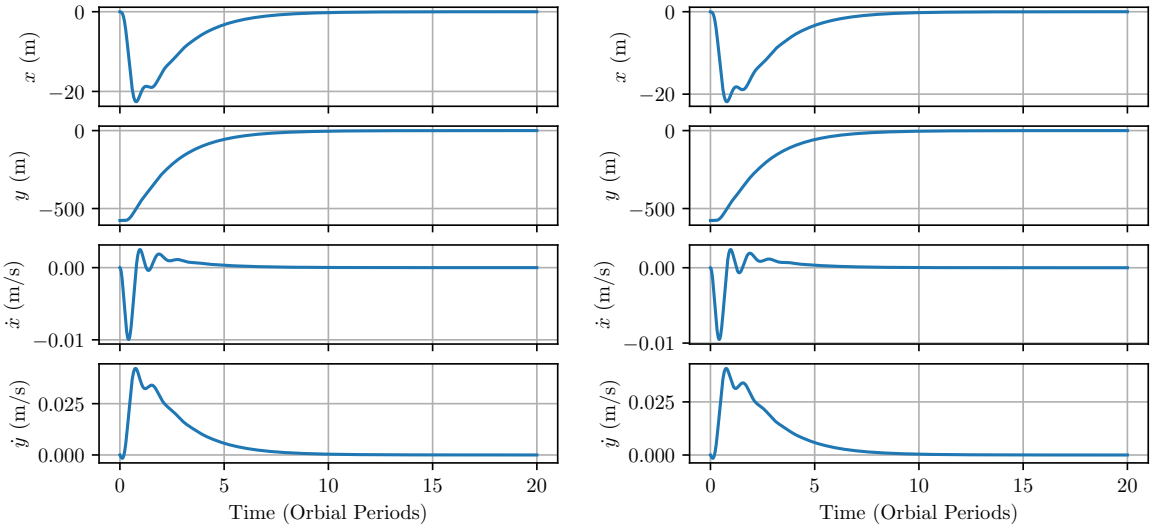

(a) LQR-Derived State Trajectory

(b) Desensitized State Trajectory

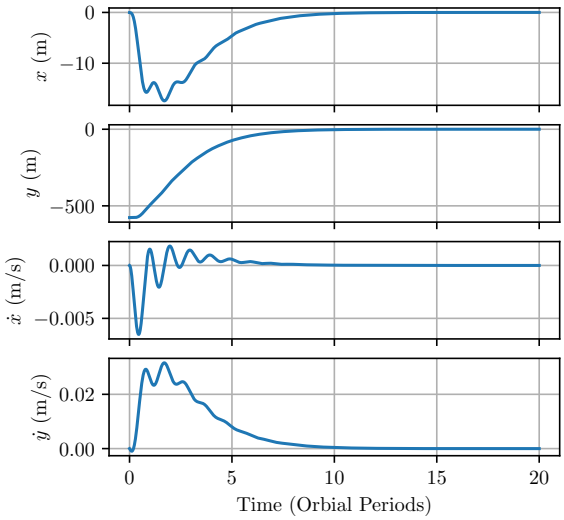

(c) Control-Desensitized State Trajectory

Figure 4: Comparison of Hill-frame relative positions using the three control types.

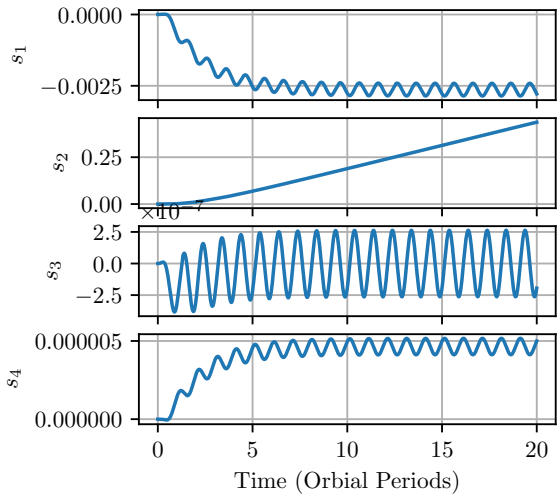

(a) LQR-Derived State Trajectory

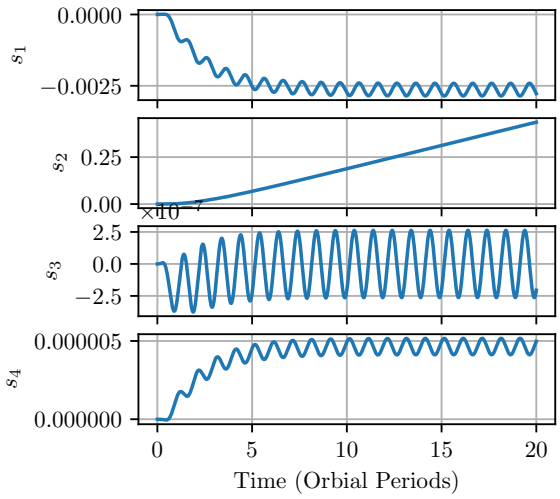

(b) Desensitized State Trajectory

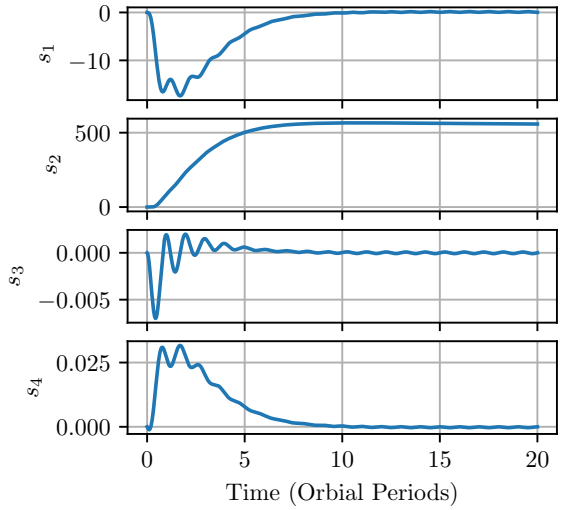

(c) Control-Desensitized State Trajectory

Figure 5: Comparison of Hill-frame relative positions using the three control types.

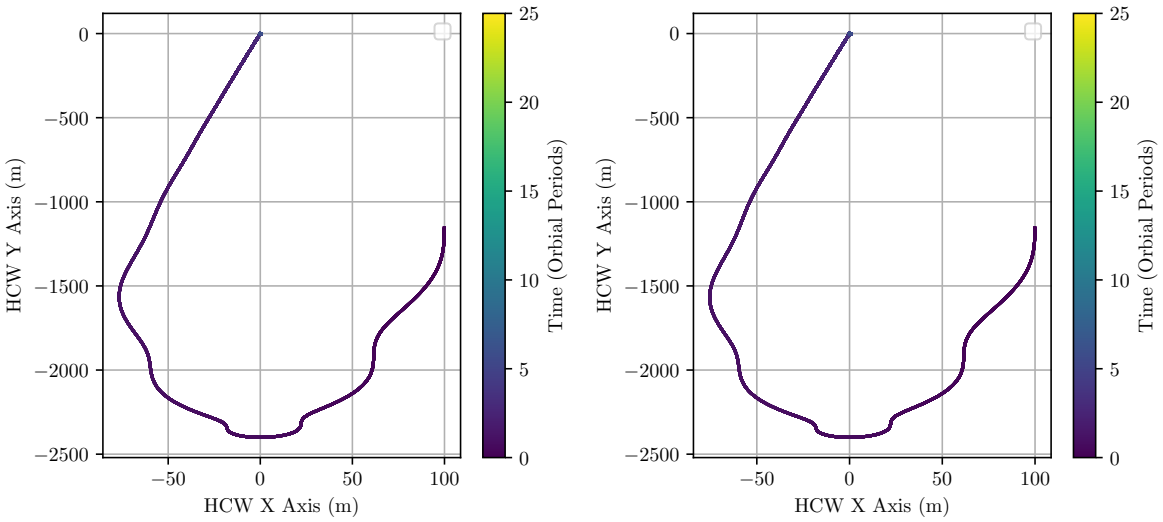

(a) LQR-Derived Hill-frame trajectory

(b) [Desensitized Trajectory

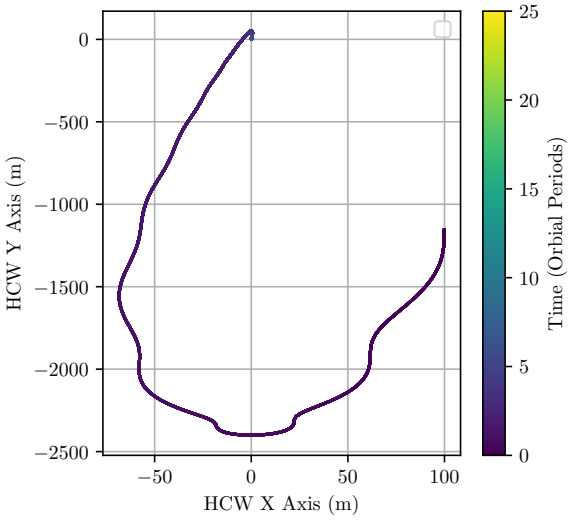

(c) Control-Desensitized Trajectory

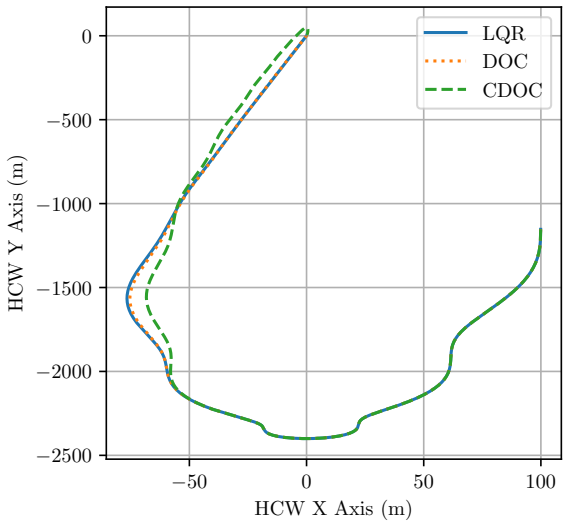

(d) Comparison of static LQR, desensitized, and control-desensitized trajectories

Figure 6: Hill-frame performance of LQR, Desensitized, and Control-Desensitized Trajectories under truth dynamics

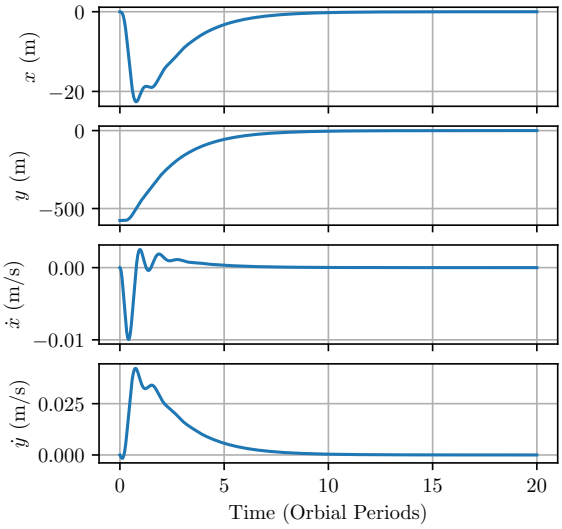

(a) LQR-Derived State Trajectory

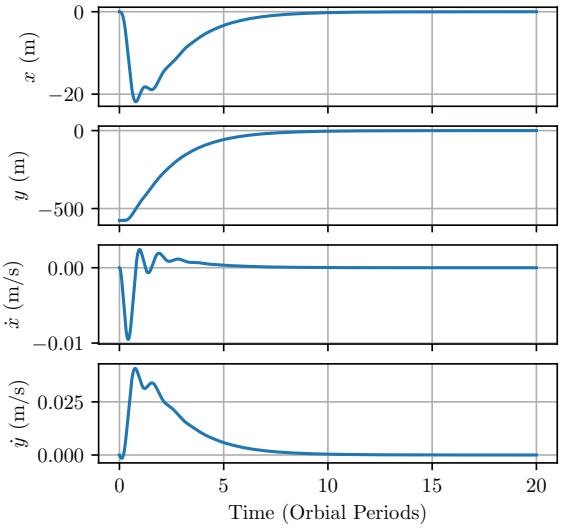

(b) Desensitized State Trajectory

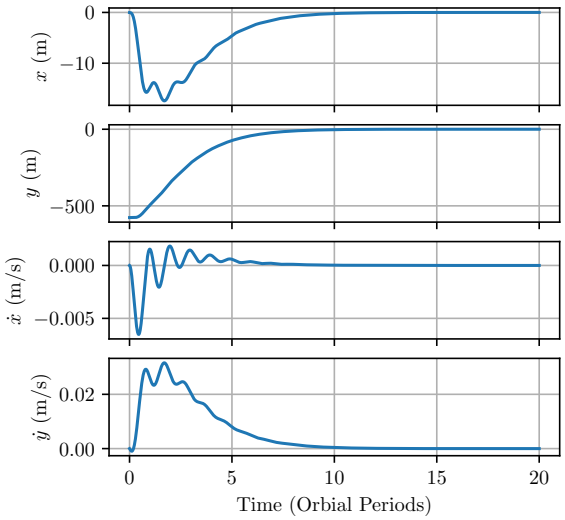

(c) Control-Desensitized State Trajectory

Figure 7: Comparison of Hill-frame relative positions using the three control types.

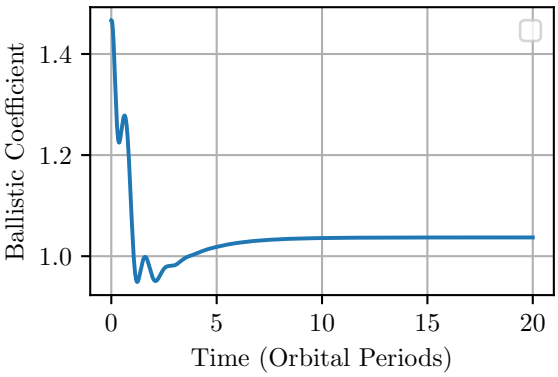

(a) LQR-Derived Ballistic Coefficient Trajectory

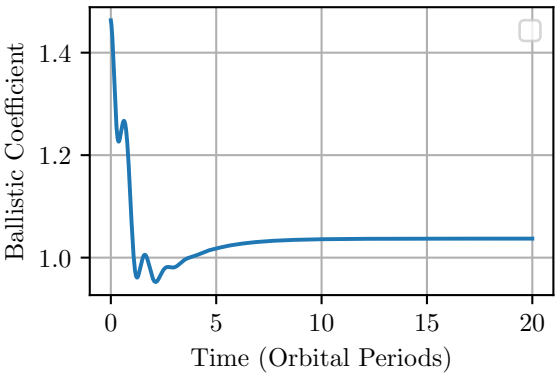

(b) Desensitized Ballistic Coefficient Trajectory

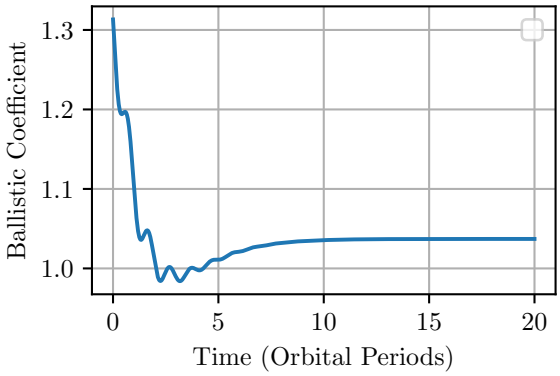

(c) Control-Desensitized Ballistic Coefficient Trajectory

Figure 8: Hill-frame performance of LQR, Desensitized, and Control-Desensitized Trajectories

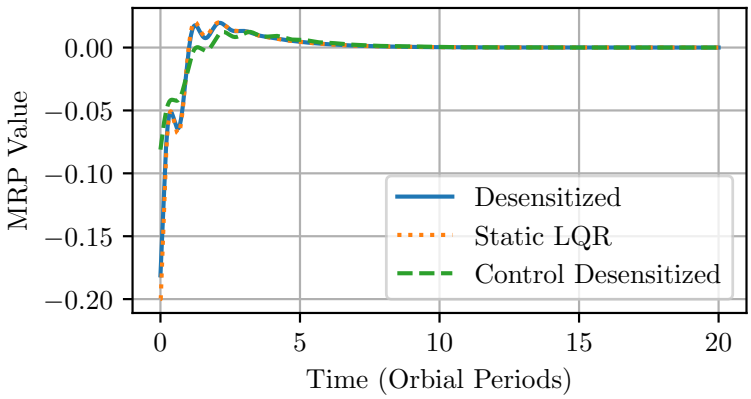

Figure 9: Attitude trajectories for each control over the maneuver.

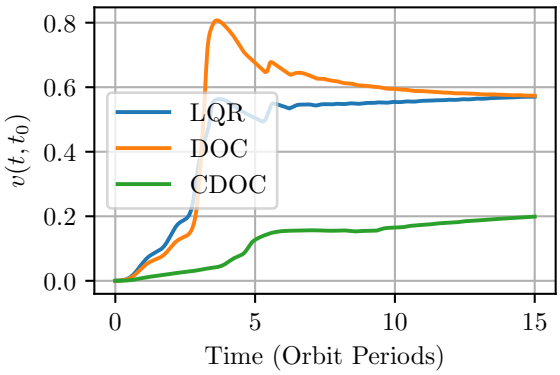

Figure 10: Nonlinearity indicies for each control type over the slot-hopping maneuver.

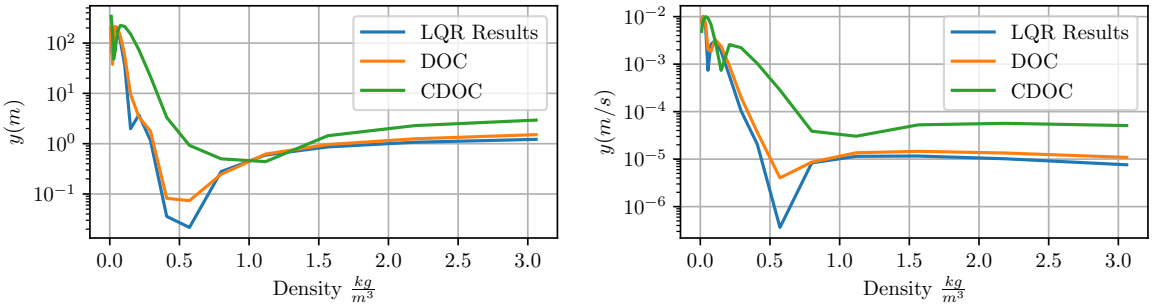

(a) Position Accuracy vs. Density

(b) Velocity Accuracy vs. Density

Figure 11: Terminal x and y states. Black lines represent the boundaries of 1,2,and 3 σ covariance ellipsoids, while orange dots represent samples. Blue dots represent the mean states. Plots are centered on the origin, and do not include all outliers.

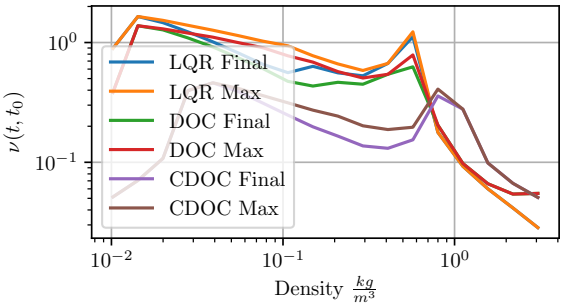

Figure 12: Terminal and maximum nonlinear indices between the nominal linear trajectory and the realized nonlinear trajectory for each system.

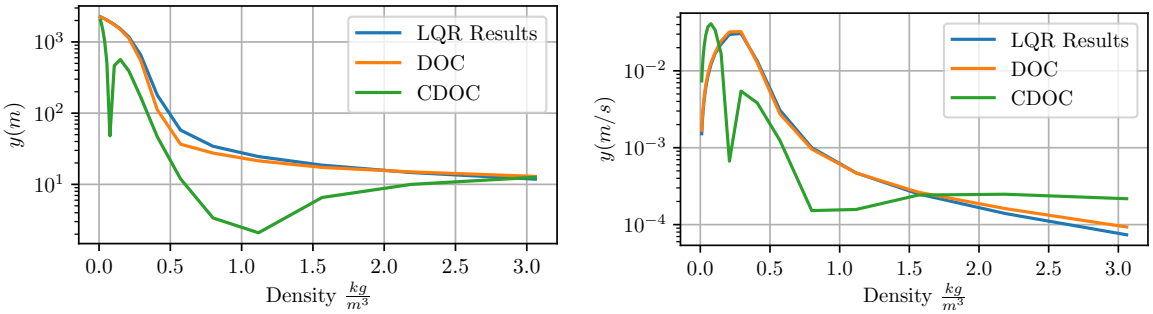

(a) Position Accuracy vs. Density

(b) Velocity Accuracy vs. Density

Figure 13: Terminal x and y states. Black lines represent the boundaries of 1,2,and 3 σ covariance ellipsoids, while orange dots represent samples. Blue dots represent the mean states. Plots are centered on the origin, and do not include all outliers.

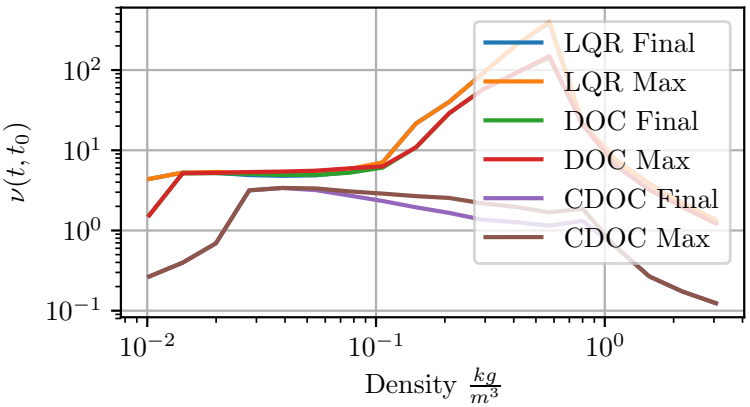

Figure 14: Terminal and maximum nonlinear indices between the nominal linear trajectory and the realized nonlinear trajectory for each system.

CONCLUSIONS

A novel strategy for applying desensitized optimal control to systems whose control inputs are functions of the sensitive parameters has been derived and compared to both traditional desensitized optimal control and finite-horizon LQR control. This strategy has then been applied to the attitude-guidance for differential drag rendezvous problem, and demonstrated in simulation $500m$. This new strategy allows mission planners to trade maneuver accuracy for predictability vis-a-vis linear simulations. Additionally, a new strategy for identifying promising cases for desensitized optimal control using standard linear controllability tools is presented to explain the results of applying control-desensitized optimal control to the nonlinear differential drag control problem.

REFERENCES

[1] Emmert, J. T., "Thermospheric mass density: A review," 2015.

[2] Marcos, F., Bowman, B., and Sheehan, R., "Accuracy of Earth's Thermospheric Neutral Density Models," *AIAA/AAS Astrodynamics Specialist Conference and Exhibit*, 2006, pp. 1–20.

[3] Mutschler, S., Axelrad, P., and Matsuo, T., "Harnessing Orbital Debris to Sense the Space Environment," 2017.

[4] Pérez, D. and Bevilacqua, R., "Differential drag spacecraft rendezvous using an Adaptive Lyapunov Control strategy," *Advances in the Astronautical Sciences*, Vol. 145, 2012, pp. 973–991.

[5] Ben-Yaacov, O. and Gurfil, P., "Long-Term Cluster Flight of Multiple Satellites Using Differential Drag," *Journal of Guidance, Control, and Dynamics*, Vol. 36, No. 6, 2013, pp. 1731–1740.

[6] Gangestad, J. W., Hardy, B. S., and Hinkley, D. A., "Operations, Orbit Determination, and Formation Control of the AeroCube-4 CubeSats," *Proceedings of the AIAA/USU Conference on Small Satellites*, Vol. SSC13, 2013, pp. SSC13–X–4.

[7] Dellelce, L. and Kerschen, G., "Optimal propellantless rendez-vous using differential drag," *Acta Astronautica*, Vol. 109, 2015, pp. 112–123.

[8] Foster, C., Hallam, H., and Mason, J., "Orbit determination and differential-drag control of Planet Labs cubesat constellations," *Advances in the Astronautical Sciences*, Vol. 156, 2016, pp. 645–657.

[9] Spiller, D., Basu, K., Curti, F., and Circi, C., "On the optimal passive formation reconfiguration by using attitude control," *Acta Astronautica*, Vol. 153, 2018.

[10] Foster, C., Mason, J., Vittaldev, V., Leung, L., Beukelaers, V., Stepan, L., and Zimmerman, R., "Constellation Phasing with Differential Drag on Planet Labs Satellites," *Journal of Spacecraft and Rockets*, Vol. 55, No. 2, 2018.

[11] Harris, A. T., Petersen, C., and Schaub, H., "Linear Coupled Attitude-Orbit Control Through Aerodynamic Forces," *2018 Space Flight Mechanics Meeting*, , No. January, 2018, pp. 1–13.

[12] Kahne, S. J., "Low-Sensitivity Design of Optimal Linear Control Systems," *IEEE Transactions on Aerospace and Electronic Systems*, Vol. AES-4, No. 3, 1968, pp. 374–379.

[13] Seywald, H., "Desensitized Optimal Trajectories," , No. November, 2016.

[14] Muenchhof, M. and Singh, T., "Desensitized Jerk Limited-Time Optimal Control of Multi-Input Systems," *Journal of Guidance, Control, and Dynamics*, Vol. 25, No. 3, 2008, pp. 474–481.

[15] Seywald, K. and Seywald, H., "Desensitized Optimal Control," , No. November, 1996.

[16] Makkapati, V. R., Dor, M., and Tsiotras, P., "Trajectory Desensitization in Optimal Control Problems," *Proceedings of the IEEE Conference on Decision and Control*, Vol. 2018-December, 2019, pp. 2478–2483.

[17] Silva, E. D., "A Formulation of the Clohessy-Wiltshire Equations to Include Dynamic Atmospheric Drag," *AIAA/AAS Astrodynamics Specialist Conference*, , No. August, 2008.